

Experimental Demonstration of Inequivalent Mutually Unbiased Bases

Wen-Zhe Yan,^{1,2,*} Yunting Li,^{3,4,5,*} Zhibo Hou,^{1,2,†} Huangjun Zhu,^{3,4,5,‡}

Guo-Yong Xiang,^{1,2,§} Chuan-Feng Li,^{1,2} and Guang-Can Guo^{1,2}

¹CAS Key Laboratory of Quantum Information, University of Science and Technology of China, Hefei 230026, People's Republic of China

²CAS Center For Excellence in Quantum Information and Quantum Physics,

University of Science and Technology of China, Hefei 230026, People's Republic of China

³State Key Laboratory of Surface Physics and Department of Physics, Fudan University, Shanghai 200433, China

⁴Institute for Nanoelectronic Devices and Quantum Computing, Fudan University, Shanghai 200433, China

⁵Center for Field Theory and Particle Physics, Fudan University, Shanghai 200433, China

(Dated: November 14, 2023)

Quantum measurements based on mutually unbiased bases (MUB) play crucial roles in foundational studies and quantum information processing. It is known that there exist inequivalent MUB, but little is known about their operational distinctions, not to say experimental demonstration. In this work, by virtue of a simple estimation problem we experimentally demonstrate the operational distinctions between inequivalent triples of MUB in dimension 4 based on high-precision photonic systems. The experimental estimation fidelities coincide well with the theoretical predictions with only 0.16% average deviation, which is 25 times less than the difference (4.1%) between the maximum estimation fidelity and the minimum estimation fidelity. Our experiments clearly demonstrate that inequivalent MUB have different information extraction capabilities and different merits for quantum information processing.

Introduction.—Quantum measurements play a key role in extracting information from quantum systems and in achieving various quantum information processing tasks, such as quantum computation, quantum communication, quantum metrology, quantum sensing, and quantum simulation [1–3]. Rank-1 projective measurements are the simplest quantum measurements discussed in most elementary textbooks on quantum mechanics. Nevertheless, their properties become elusive if we consider two or more projective measurements. Since each rank-1 projective measurement is tied to an orthonormal basis, and vice versa, the study of rank-1 projective measurements is intertwined with the study of orthonormal bases.

Two rank-1 projective measurements are *mutually unbiased* or complementary if the outcome of one measurement is completely random whenever the outcome of the other measurement is certain. The corresponding bases are called *mutually unbiased bases* (MUB) [4–7]. MUB are closely tied to the complementarity principle [8] and uncertainty relations [9–13], which play key roles in quantum mechanics. Moreover, MUB have found numerous applications in quantum information processing, including quantum cryptography [7, 13–15], quantum random access codes [16, 17], quantum state estimation [5, 6, 18–20], and quantum verification [21, 22].

Two sets of MUB are (unitarily) *equivalent* if they can be turned into each other by unitary transformations up to the order of basis elements and overall phase factors. Otherwise, they are *inequivalent*. Inequivalent MUB exist in certain dimensions at least four [23], and this intriguing phenomenon has attracted the attention of many researchers in various research areas [7, 15–17, 23–27]. However, little is known about the operational distinc-

tions between inequivalent MUB, and there is no experimental demonstration before as far as we know.

As notable exceptions, Aguilar et al. showed that inequivalent MUB can achieve different success probabilities in quantum random access codes [16]. Designolle et al. showed that inequivalent MUB may have different degrees of measurement incompatibility as quantified by the noise robustness [25]. Hiesmayr et al. showed that some MUB are more effective than others in detecting entanglement [26]. It is not clear whether these results can be demonstrated in experiments in the near future. Very recently, starting from a simple estimation problem, one of the authors showed that inequivalent MUB may have different information-extraction capabilities and can be distinguished by the *estimation fidelity* [27], which is amenable to experimental demonstration.

In this work, using photonic systems we experimentally demonstrate the operational distinctions between inequivalent triples of MUB in dimension 4 based on a simple three-copy estimation problem. To this end, we use polarization and path degrees of freedom of a photon to form a ququad. Then we implement a three-copy estimation protocol in which the projective measurements are determined by triples of MUB, so that the estimation fidelities are tied to the intrinsic properties of MUB. The projective measurements we realized have average fidelity above 0.995. The experimental estimation fidelities coincide well with the theoretical predictions with only 0.16% average deviation, which is 25 times less than the difference (4.1%) between the maximum estimation fidelity and the minimum estimation fidelity. In this way, our experiments clearly demonstrate different information extraction capabilities of inequivalent MUB, which

has never been demonstrated before.

A simple estimation problem.—Suppose a quantum device can prepare N copies of a random pure quantum state ρ on a d -dimensional Hilbert space \mathcal{H} according to the Haar measure. We are asked to estimate the identity of ρ as accurately as possible as quantified by the average fidelity. If we perform the quantum measurement characterized by the positive operator-valued measure (POVM) $\mathcal{A} = \{A_j\}_j$ on $\rho^{\otimes N}$, then the probability of obtaining outcome A_j is $p_j = \text{tr}(\rho^{\otimes N} A_j)$. Let $\hat{\rho}_j$ be the estimator corresponding to outcome j . Let P_{N+1} be the projector onto the symmetric subspace in $\mathcal{H}^{\otimes(N+1)}$ and $D_{N+1} = \text{tr}(P_{N+1})$. Then the average fidelity reads [27]

$$\begin{aligned} \bar{F} &= \sum_j \int d\rho p_j \text{tr}(\rho \hat{\rho}_j) = \frac{\sum_j \text{tr}[Q(A_j) \hat{\rho}_j]}{(N+1)! D_{N+1}} \\ &\leq F(\mathcal{A}) := \sum_j \frac{\|Q(A_j)\|}{(N+1)! D_{N+1}}, \end{aligned} \quad (1)$$

where the integration is over the set of all pure states with Haar measure and

$$Q(A_j) := (N+1)! \text{tr}_{1,\dots,N}[P_{N+1}(A_j \otimes 1)]. \quad (2)$$

The upper bound in Eq. (1) is saturated iff each estimator $\hat{\rho}_j$ is supported in the eigenspace of $Q(A_j)$ associated with the largest eigenvalue. Here $F(\mathcal{A})$ is the maximum average fidelity that can be achieved by the POVM \mathcal{A} and is called the *estimation fidelity* [27]. It encodes valuable information about the POVM and is pretty useful for understanding elementary quantum measurements.

In the above analysis, the ensemble of Haar random pure states can be replaced by any ensemble of pure states that forms a t -design with $t = N+1$, which might be more appealing to practical applications. Recall that a set of K states $\{|\psi_j\rangle\}_j$ in \mathcal{H} is a t -design if $\sum_j (|\psi_j\rangle\langle\psi_j|)^{\otimes t}$ is proportional to the projector P_t onto the symmetric subspace in $\mathcal{H}^{\otimes t}$ [28–30] or, equivalently, if the t th *frame potential*

$$\Phi_t(\{|\psi_j\rangle\}_j) := \frac{1}{K^2} \sum_{j,k} |\langle\psi_j|\psi_k\rangle|^{2t} \quad (3)$$

saturates the inequality $\Phi_t(\{|\psi_j\rangle\}_j) \geq 1/D_t$.

Distinguishing inequivalent MUB.—Here we are particularly interested in inequivalent triples of MUB in dimension 4, which can be distinguished by the three-copy estimation fidelity [27] as illustrated in Fig. 1. The three bases are denoted by $\{|\alpha_j\rangle\}_j$, $\{|\beta_j\rangle\}_j$, and $\{|\gamma_j\rangle\}_j$, respectively, where $j = 1, 2, 3, 4$; the corresponding rank-1 projective measurements read $\mathcal{A} = \{|\alpha_j\rangle\langle\alpha_j|\}_j$, $\mathcal{B} = \{|\beta_j\rangle\langle\beta_j|\}_j$, and $\mathcal{C} = \{|\gamma_j\rangle\langle\gamma_j|\}_j$. To be specific, the first basis is chosen as the computational basis; the second and third bases correspond to the columns of the two

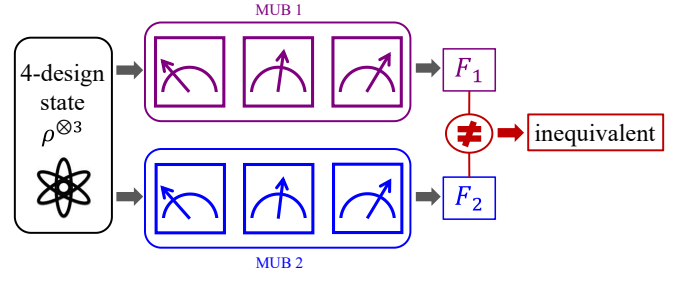


FIG. 1. The basic idea for distinguishing inequivalent triples of MUB. After preparing three copies of each state ρ in a given 4-design and performing three projective measurements associated with each triple of MUB, the fidelity between the optimal estimator $\hat{\rho}$ and ρ is evaluated. The estimation fidelity of each MUB is determined by averaging the fidelity $\text{tr}(\rho \hat{\rho})$ over the 4-design and many repetitions. Two MUB are inequivalent if their estimation fidelities are different.

Hadamard matrices, respectively [23, 27]:

$$\begin{aligned} H_{\mathcal{B}} &= \frac{1}{2} \begin{pmatrix} 1 & 1 & 1 & 1 \\ 1 & ie^{ix} & -1 & -ie^{ix} \\ 1 & -1 & 1 & -1 \\ 1 & -ie^{ix} & -1 & ie^{ix} \end{pmatrix}, \\ H_{\mathcal{C}} &= \frac{1}{2} \begin{pmatrix} 1 & 1 & 1 & 1 \\ -e^{iy} & e^{iz} & e^{iy} & -e^{iz} \\ 1 & -1 & 1 & -1 \\ e^{iy} & e^{iz} & -e^{iy} & -e^{iz} \end{pmatrix}, \end{aligned} \quad (4)$$

where $x, y, z \in [0, \pi]$ are three real parameters. By construction, it is easy to verify that

$$|\langle\alpha_j|\beta_k\rangle|^2 = |\langle\beta_k|\gamma_l\rangle|^2 = |\langle\alpha_j|\gamma_l\rangle|^2 = \frac{1}{4} \quad (5)$$

for $j, k, l = 1, 2, 3, 4$. So the three bases for given x, y, z are indeed mutually unbiased. As shown in Ref. [27], the estimation fidelity $F_{\text{MUB}}(x, y, z) := F(\mathcal{A} \otimes \mathcal{B} \otimes \mathcal{C})$ can be used to distinguish inequivalent MUB. Moreover, the difference between the maximum and minimum estimation fidelities is about 4.1%, which is amenable to experimental demonstration.

To determine the estimation fidelity in experiments, we prepare three copies of each ququad state ρ_i from a given 4-design composed of K states and perform the three projective measurements \mathcal{A}, \mathcal{B} , and \mathcal{C} , respectively. If the outcomes j, k, l are obtained, then we construct an estimator $\hat{\rho}_{jkl}$ on the eigenspace of $\mathcal{Q}(|\alpha_j\rangle\langle\alpha_j| \otimes |\beta_k\rangle\langle\beta_k| \otimes |\gamma_l\rangle\langle\gamma_l|)$ corresponding to the largest eigenvalue and evaluate its fidelity with ρ_i . To suppress statistical fluctuation, the same measurements are repeated M times for each state ρ_i in the 4-design. Denote by $\hat{\rho}_{im}$ the m th estimator for the i th state ρ_i , where $m = 1, 2, \dots, M$ and $i = 1, 2, \dots, K$. Then the estimation fidelity is calculated as follows:

$$F_{\text{MUB}}(x, y, z) = \frac{1}{KM} \sum_i \sum_m \text{tr}(\rho_i \hat{\rho}_{im}). \quad (6)$$

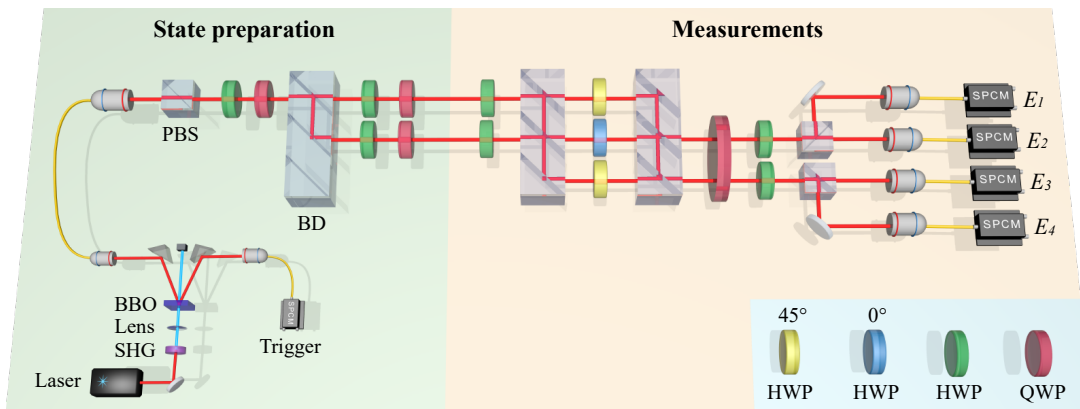


FIG. 2. Experimental setup. The module of state preparation generates a single photon using the type-II phase-matched spontaneous parametric down-conversion (SPDC) process and prepares the desired ququad state in polarization and path degrees of freedom. The measurement module implements one of the three projective measurements \mathcal{A} , \mathcal{B} , and \mathcal{C} associated with a triple of MUB. The four detectors at positions E_1 to E_4 correspond to the four outcomes of the measurement. Key elements include PBS (polarizing beam splitter), HWP (half wave plate), QWP (quarter wave plate), and BD (beam displacer). The wave plates which have not been marked with specific angles are the ones that need to be rotated during the experiments.

To facilitate experimental realization, we constructed two 4-designs with small cardinalities in dimension 4. The first 4-design is constructed from an orbit of length 960 of the restricted Clifford group and is referred to as the *Clifford 4-design* henceforth. By contrast, the full Clifford orbit has length 3840 (see Secs. S1 and S2 in the Supplemental Material [31]). This theoretical result is of independent interest, given that the Clifford group is only a 3-design, and the restricted Clifford group is only a 2-design [32–35]. The second one is a (approximate) *numerical 4-design* composed of 200 states, which is generated using the optimization algorithm in Refs. [36, 37] (see Sec. S3 in the Supplemental Material [31]).

Experimental setup.—The experimental setup for realizing the three-copy estimation protocol is illustrated in Fig. 2. We use the polarization (horizontal H and vertical V) and the path (up and down) degrees of freedom of a single photon to form a ququad. The setup is composed of two modules: the state preparation module, which can generate an arbitrary ququad state, and the measurement module, which can perform one of the projective measurements \mathcal{A} , \mathcal{B} , and \mathcal{C} .

In the state preparation process, a light pulse with a central wavelength of 780 nm first passes through a frequency doubler. Then the ultraviolet pulse is focused onto a BBO crystal cut for the type-II phase-matched spontaneous parametric down-conversion (SPDC) process to create a pair of photons. One photon is detected by a single-photon-counting module (SPCM) as a trigger, while the other acts as a heralded single-photon source. The single photon is initialized in H polarization by a polarizing beam splitter (PBS). Any polarization state can be generated by a combination of a half-wave plate (HWP) and a quarter-wave plate (QWP). A beam displacer (BD) which separates the H component and V

component by 4 mm transforms this polarization state into a path state. The following two combinations of a HWP and a QWP adjust the polarization states in the two paths so as to generate the desired ququad state. Then, the state is sent into the measurement module, which performs one of the projective measurements \mathcal{A} , \mathcal{B} , and \mathcal{C} (see Sec. S4 in the Supplemental Material [31]). The regulation of the parameters x, y, z featuring in \mathcal{B} and \mathcal{C} is realized by changing the rotation angles of some HWPs. Four SPCMs at the end correspond to four outcomes of the measurement.

Experimental results.—In our experiment, we considered 18 triples of MUB corresponding to the parameters $x = \pi/2$, $y \in \{0, \pi/2\}$, and $z \in \{0, \pi/8, \pi/4, \dots, \pi\}$, which share the two bases \mathcal{A} and $\mathcal{B}(x = \pi/2)$. To characterize each projective measurement that was actually realized, we sent 36 states, the tensor products of the six eigenstates of three Pauli operators, to the measurement device and performed quantum measurement tomography. Each state was prepared and measured 10000 times. Then the four projectors were reconstructed from the measurement statistics using the method in Ref. [38] and the overall fidelity was evaluated as in Ref. [39]. This procedure was repeated 10 times to determine the mean fidelity and error bar (standard deviation). Overall fidelities of the realized measurements for \mathcal{A} and $\mathcal{B}(x = \pi/2)$ are 0.9990 ± 0.0001 and 0.9977 ± 0.0003 , respectively, while those for $\mathcal{C}(y, z)$ are shown in Table I. The average overall fidelity of these measurements is above 0.995, demonstrating that they were realized with high quality.

Next, we implemented the three-copy estimation protocol to determine the estimation fidelity $F_{\text{MUB}}(x, y, z)$. To this end, we prepared three copies of each state in the Clifford 4-design and performed the three projective mea-

TABLE I. Overall fidelity of the measurement $\mathcal{C}(y, z)$ realized in the experiment. Each fidelity value is the average over 10 repeated reconstructions. The error bar indicates the standard deviation of 10 repetitions.

z	0	$\pi/8$	$\pi/4$	$3\pi/8$	$\pi/2$	$5\pi/8$	$3\pi/4$	$7\pi/8$	π
$\mathcal{C}(y = \pi/2)$	0.9979(2)	0.9966(4)	0.9943(12)	0.9962(8)	0.9975(8)	0.9966(10)	0.9948(8)	0.9956(7)	0.9975(4)
$\mathcal{C}(y = 0)$	0.9977(3)	0.9965(7)	0.9938(10)	0.9959(10)	0.9976(2)	0.9954(12)	0.9939(7)	0.9947(10)	0.9978(4)

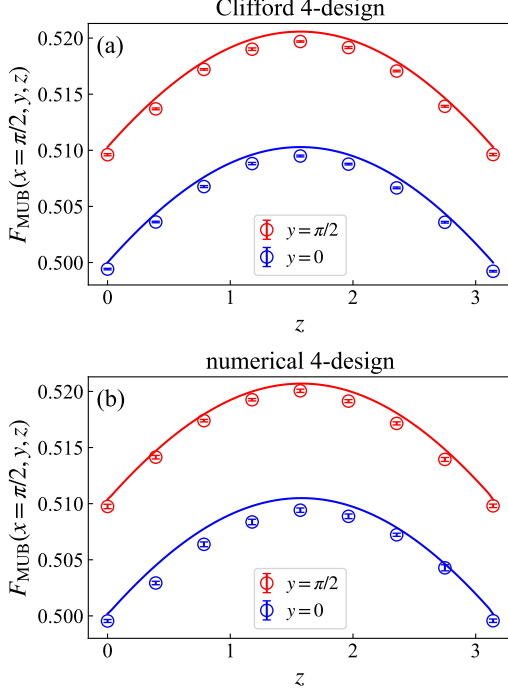


FIG. 3. Experimental results (circles with error bars) and theoretical predictions (solid lines) on the three-copy estimation fidelity $F_{\text{MUB}}(x, y, z) = F(\mathcal{A} \otimes \mathcal{B} \otimes \mathcal{C})$ based on the Clifford 4-design (a) and numerical 4-design (b), respectively. The error bars indicate the standard deviations of 10 repeated experiments.

TABLE II. Average and maximum deviations between experimental (three-copy and two-copy) estimation fidelities and theoretical predictions based on the Clifford 4-design and numerical 4-design, respectively.

	4-design	average	maximum
three-copy	Clifford	0.0008	0.0010
	numerical	0.0008	0.0016
two-copy	Clifford	0.0007	0.0013
	numerical	0.0009	0.0019

measurements \mathcal{A} , $\mathcal{B}(x = \pi/2)$, and $\mathcal{C}(y, z)$, respectively. To suppress statistical fluctuation and determine the error bar, the preparation and measurement procedure were repeated 10000×10 times. For simplicity, we share the measurement outcomes of \mathcal{A} and $\mathcal{B}(x = \pi/2)$ for all 18 sets of MUB. The estimation fidelity $F_{\text{MUB}}(x, y, z)$ cal-

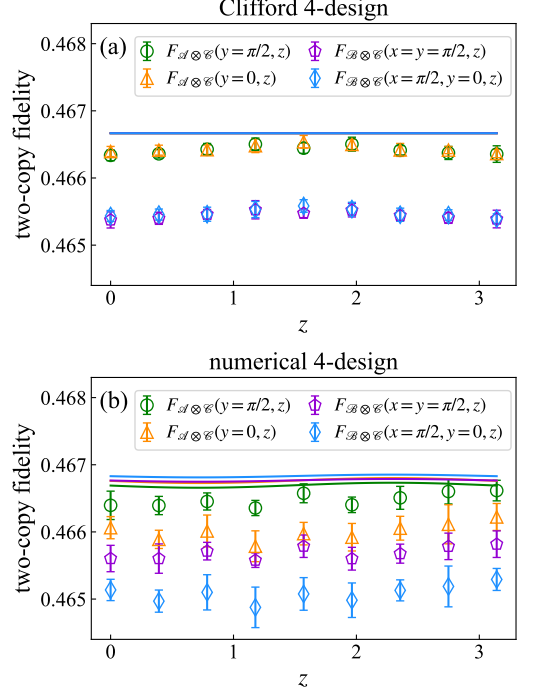


FIG. 4. Experimental results (markers with error bars) and theoretical predictions (solid lines) on the two-copy estimation fidelities achieved by the product measurements $\mathcal{A} \otimes \mathcal{C}$ and $\mathcal{B} \otimes \mathcal{C}$ based on the Clifford 4-design (a) and numerical 4-design (b), respectively. The error bars indicate the standard deviations of 10 repeated experiments.

culated by Eq. (6) are shown in plot (a) in Fig. 3. The experimental results (circles with error bars) coincide well with the theoretical predictions (solid lines). This claim is further corroborated by Table II, which shows the average and maximum deviations between experiments and theory. The experimental errors mainly come from the instability and drift of the phases of the Mach-Zehnder interferometers. Figure 3 clearly delineates the variation of the estimation fidelity with the parameters y, z for $x = \pi/2$, which highlights the operational distinction between inequivalent MUB. Notably, the estimation fidelity reaches the maximum 0.5197 at $x = y = z = \pi/2$ and the minimum 0.4992 at $x = \pi/2, y = 0, z = \pi$; the difference 0.0205 is 25 times larger than the average deviation shown in Table II.

Next, we implemented the three-copy estimation protocol based on the numerical 4-design instead of the Clif-

ford 4-design. The results shown in plot (b) in Fig. 3 and Table II are quite similar to the counterparts based on the Clifford 4-design, although the two 4-designs are very different. These results further demonstrate that the operational distinction between inequivalent MUB is independent of the choice of 4-designs. Incidentally, inequivalent triples of MUB in dimension 4 cannot be distinguished by noise robustness considered in Ref. [25], which manifests the advantage of our approach.

As comparison, the two-copy estimation fidelity achieved by any product measurement based on MUB equals 0.4667 [27], assuming that the state ensemble forms an ideal 4-design. Note that inequivalent MUB cannot be distinguished by the two-copy estimation fidelity, which provides information only about pairwise overlaps of the basis states [27]. To demonstrate this result, we reprocessed the experimental data to determine the two-copy estimation fidelity. The experimental two-copy estimation fidelities achieved by $\mathcal{A} \otimes \mathcal{B}(x = \pi/2)$ are 0.4664 ± 0.0001 and 0.4668 ± 0.0001 based on the Clifford 4-design and numerical 4-design, respectively, while those for $\mathcal{A} \otimes \mathcal{C}$ and $\mathcal{B} \otimes \mathcal{C}$ are shown in Fig. 4 together with theoretical predictions. The average and maximum deviations are shown in Table II. Again, the experimental results agree very well with theoretical predictions even if the numerical 4-design is not ideal.

Summary.—In this work, we implemented a three-copy estimation protocol to demonstrate the operational distinction between inequivalent MUB. In our experiments, we used polarization and path degrees of freedom of a photon to form a ququad and performed projective measurements associated with 18 triples of MUB in dimension 4 with high quality. The experimental estimation fidelities agree well with theoretical predictions with only 0.16% average deviation, which is accurate enough to distinguish inequivalent MUB. Our experiments clearly demonstrate that inequivalent MUB may have different information extraction capabilities, which have operational consequences. These results are of intrinsic interest not only to foundational studies, but also to many tasks in quantum information processing, such as quantum state estimation, entanglement detection, and quantum communication.

The work at the University of Science and Technology of China is supported by the National Natural Science Foundation of China (Grants Nos. 62222512, 12104439, 12134014, and 11974335), the Anhui Provincial Natural Science Foundation (Grant No. 2208085J03), USTC Research Funds of the Double First-Class Initiative (Grant Nos. YD2030002007 and YD2030002011) and the Fundamental Research Funds for the Central Universities (Grant No. WK2470000035). The work at Fudan University is supported by the National Natural Science Foundation of China (Grant No. 92165109), National Key Research and Development Program of China (Grant No. 2022YFA1404204), and Shanghai Mu-

nicipal Science and Technology Major Project (Grant No. 2019SHZDZX01).

* These authors contributed equally to this work.

† houzhibo@ustc.edu.cn

‡ zhuhuangjun@fudan.edu.cn

§ gyxiang@ustc.edu.cn

- [1] J. von Neumann, *Mathematical Foundations of Quantum Mechanics* (Princeton University Press, 2018) translated from the German edition by R. T. Beyer.
- [2] M. A. Nielsen and I. L. Chuang, *Quantum Computation and Quantum Information: 10th Anniversary Edition* (Cambridge University Press, 2010).
- [3] P. Busch, P. J. Lahti, J.-P. Pellonpää, and K. Ylänen, *Quantum measurement* (Springer, Switzerland, 2016).
- [4] J. Schwinger, Unitary operator bases, Proc. Natl. Acad. Sci. **46**, 570 (1960).
- [5] I. D. Ivonovic, Geometrical description of quantal state determination, J. Phys. A: Math. Gen. **14**, 3241 (1981).
- [6] W. K. Wootters and B. D. Fields, Optimal state-determination by mutually unbiased measurements, Ann. Phys. (N. Y.) **191**, 363 (1989).
- [7] T. Durt, B.-G. Englert, I. Bengtsson, and K. Życzkowski, On mutually unbiased bases, Int. J. Quantum Inf. **08**, 535 (2010).
- [8] N. Bohr, The quantum postulate and the recent development of atomic theory, Nature **121**, 580 (1928).
- [9] W. Heisenberg, Über den anschaulichen inhalt der quantentheoretischen kinematik und mechanik, Zeitschrift für Physik **43**, 172 (1927).
- [10] H. P. Robertson, The uncertainty principle, Phys. Rev. **34**, 163 (1929).
- [11] P. Busch, P. Lahti, and R. F. Werner, Colloquium: Quantum root-mean-square error and measurement uncertainty relations, Rev. Mod. Phys. **86**, 1261 (2014).
- [12] S. Wehner and A. Winter, Entropic uncertainty relations—a survey, New J. Phys. **12**, 025009 (2010).
- [13] P. J. Coles, M. Berta, M. Tomamichel, and S. Wehner, Entropic uncertainty relations and their applications, Rev. Mod. Phys. **89**, 015002 (2017).
- [14] D. Mayers and A. Yao, Quantum cryptography with imperfect apparatus, in *Proceedings 39th Annual Symposium on Foundations of Computer Science* (1998) pp. 503–509.
- [15] A. Tavakoli, M. Farkas, D. Rosset, J.-D. Bancal, and J. Kaniewski, Mutually unbiased bases and symmetric informationally complete measurements in Bell experiments, Sci. Adv. **7**, eabc3847 (2021).
- [16] E. A. Aguilar, J. J. Borkala, P. Mironowicz, and M. Pawłowski, Connections between mutually unbiased bases and quantum random access codes, Phys. Rev. Lett. **121**, 050501 (2018).
- [17] M. Farkas and J. Kaniewski, Self-testing mutually unbiased bases in the prepare-and-measure scenario, Phys. Rev. A **99**, 032316 (2019).
- [18] A. Roy and A. J. Scott, Weighted complex projective 2-designs from bases: Optimal state determination by orthogonal measurements, J. Math. Phys. **48**, 072110 (2007).
- [19] H. Zhu, Quantum state estimation with informationally

- overcomplete measurements, *Phys. Rev. A* **90**, 012115 (2014).
- [20] R. B. A. Adamson and A. M. Steinberg, Improving quantum state estimation with mutually unbiased bases, *Phys. Rev. Lett.* **105**, 030406 (2010).
- [21] Z. Li, Y.-G. Han, and H. Zhu, Efficient verification of bipartite pure states, *Phys. Rev. A* **100**, 032316 (2019).
- [22] H. Zhu and M. Hayashi, Optimal verification and fidelity estimation of maximally entangled states, *Phys. Rev. A* **99**, 052346 (2019).
- [23] S. Brierley, S. Weigert, and I. Bengtsson, All mutually unbiased bases in dimensions two to five, *Quantum Inf. Comput.* **10**, 803 (2009).
- [24] W. M. Kantor, MUBs inequivalence and affine planes, *J. Math. Phys.* **53**, 032204 (2012).
- [25] S. Designolle, P. Skrzypczyk, F. Fröwis, and N. Brunner, Quantifying measurement incompatibility of mutually unbiased bases, *Phys. Rev. Lett.* **122**, 050402 (2019).
- [26] B. C. Hiesmayr, D. McNulty, S. Baek, S. S. Roy, J. Bae, and D. Chruściński, Detecting entanglement can be more effective with inequivalent mutually unbiased bases, *New J. Phys.* **23**, 093018 (2021).
- [27] H. Zhu, Quantum measurements in the light of quantum state estimation, *PRX Quantum* **3**, 030306 (2022).
- [28] J. M. Renes, R. Blume-Kohout, A. J. Scott, and C. M. Caves, Symmetric informationally complete quantum measurements, *J. Math. Phys.* **45**, 2171 (2004).
- [29] G. Zauner, Quantum designs: Foundations of a noncommutative design theory, *Int. J. Quantum Inf.* **09**, 445 (2011).
- [30] A. J. Scott, Tight informationally complete quantum measurements, *J. Phys. A: Math. Gen.* **39**, 13507 (2006).
- [31] See Supplemental Material for the details.
- [32] D. Gottesman, Stabilizer codes and quantum error correction (1997), arXiv:quant-ph/9705052.
- [33] H. Zhu, Multiqubit Clifford groups are unitary 3-designs, *Phys. Rev. A* **96**, 062336 (2017).
- [34] Z. Webb, The Clifford group forms a unitary 3-design, *Quantum Info. Comput.* **16**, 1379–1400 (2016).
- [35] H. Zhu, R. Kueng, M. Grassl, and D. Gross, The Clifford group fails gracefully to be a unitary 4-design (2016), arXiv:1609.08172.
- [36] D. Hughes and S. Waldron, Spherical (t, t) -designs with a small number of vectors, *Linear Algebra and its Applications* **608**, 84 (2021).
- [37] A. Elzenaar, <https://github.com/aelzenaar/tightframes>.
- [38] J. Fiurášek, Maximum-likelihood estimation of quantum measurement, *Phys. Rev. A* **64**, 024102 (2001).
- [39] Z. Hou, J.-F. Tang, J. Shang, H. Zhu, J. Li, Y. Yuan, K.-D. Wu, G.-Y. Xiang, C.-F. Li, and G.-C. Guo, Deterministic realization of collective measurements via photonic quantum walks, *Nat. Commun.* **9**, 1414 (2018).

Experimental Demonstration of Inequivalent Mutually Unbiased Bases: Supplemental Material

S1. THE CLIFFORD GROUP AND RESTRICTED CLIFFORD GROUP

The Pauli group for one qubit is generated by the following three Pauli matrices:

$$X = \begin{pmatrix} 0 & 1 \\ 1 & 0 \end{pmatrix}, \quad Y = \begin{pmatrix} 0 & -i \\ i & 0 \end{pmatrix}, \quad Z = \begin{pmatrix} 1 & 0 \\ 0 & -1 \end{pmatrix}. \quad (\text{S1})$$

The n -qubit Pauli group \mathcal{P}_n is composed of the n -fold tensor products of Pauli matrices and the identity $\{I, X, Y, Z\}^{\otimes n}$ together with the phase factors $\{\pm 1, \pm i\}$, which has order 4^{n+1} by construction. In many applications, the overall phases are irrelevant, and it is more convenient to work with the Pauli group \mathcal{P}_n modulo phase factors, which is also called the Pauli group (also known as the projective Pauli group) and is denoted by $\bar{\mathcal{P}}_n$ to distinguish it from \mathcal{P}_n . For the convenience of discussion, the group $\bar{\mathcal{P}}_n$ can be identified with the set $\{I, X, Y, Z\}^{\otimes n}$.

The Clifford group \mathcal{C}_n is the normalizer of the Pauli group \mathcal{P}_n [1–3]. In other words, it is composed of all unitary operators that map the group \mathcal{P}_n to itself. The Clifford group modulo overall phase factors is also called the Clifford group and is denoted by $\bar{\mathcal{C}}_n$ in analogy to the Pauli group $\bar{\mathcal{P}}_n$. The group $\bar{\mathcal{C}}_n$ can be generated by phase gates P , Hadamard gates H for individual qubits and controlled-not (CNOT) gates for all pairs of qubits [3], where

$$P = \begin{pmatrix} 1 & 0 \\ 0 & i \end{pmatrix}, \quad H = \frac{1}{\sqrt{2}} \begin{pmatrix} 1 & 1 \\ 1 & -1 \end{pmatrix}, \quad \text{CNOT} = \begin{pmatrix} 1 & 0 & 0 & 0 \\ 0 & 1 & 0 & 0 \\ 0 & 0 & 0 & 1 \\ 0 & 0 & 1 & 0 \end{pmatrix}. \quad (\text{S2})$$

The quotient group $\bar{\mathcal{C}}_n/\bar{\mathcal{P}}_n$ is isomorphic to the symplectic group $\text{Sp}(2n, 2)$, which is the group of linear transformations (symplectic matrices) on \mathbb{F}_2^{2n} that preserve the standard symplectic inner product [1, 2].

In this work, we focus on the two-qubit Clifford group with $n = 2$. In this case, the symplectic group $\text{Sp}(4, 2)$ is isomorphic to the symmetric group of six letters and has order 720. Accordingly, the Clifford group $\bar{\mathcal{C}}_2$ has order 11520. In addition, we are particularly interested in a special subgroup of the Clifford group, the restricted Clifford group $\bar{\mathcal{C}}_2^r$ [4], whose quotient over the Pauli group is isomorphic to $\text{SL}(2, 4)$, which in turn is isomorphic to the alternating group A_5 . Both $\text{SL}(2, 4)$ and A_5 have orders 60, so $\bar{\mathcal{C}}_2^r$ has order 960. To be specific, $\bar{\mathcal{C}}_2^r$ is generated by the following two unitary operators:

$$H_2 \text{CNOT}_{12} P_1 H_2, \quad H_1 P_2 \text{CNOT}_{12} H_2, \quad (\text{S3})$$

where H_j and P_j for $j = 1, 2$ denote the Hadamard gate and phase gate acting on the j th qubit, and CNOT_{12} is the CNOT gate with the first qubit as the control qubit and the second qubit as the target qubit.

S2. CONSTRUCTING 4-DESIGNS FROM (RESTRICTED) CLIFFORD ORBITS

Although the Clifford group is a 3-design, but not a 4-design [4, 5], its orbits may form 4-designs if we choose suitable fiducial states [6]. In the case of two qubits under consideration, we can even construct a 4-design from certain orbit of the restricted Clifford group, which is only a 2-design [4].

Here we focus on product fiducial states of the form $|\psi(\frac{1}{\sqrt{3}}, \frac{1}{\sqrt{3}}, \frac{1}{\sqrt{3}})\rangle \otimes |\psi(r_1, r_2, r_3)\rangle$, where each qubit state is characterized by its Bloch vector. According to Ref. [6], the orbit generated by the Clifford group forms a 4-design iff the Bloch vector (r_1, r_2, r_3) satisfies the following condition [6]:

$$r_1^4 + r_2^4 + r_3^4 = \frac{5}{7}. \quad (\text{S4})$$

The Bloch vector can also be represented by two spherical angles θ, ϕ via the relation $(\sin \theta \cos \phi, \sin \theta \sin \phi, \cos \theta) = (r_1, r_2, r_3)$. Then the condition in Eq. (S4) can be expressed as follows,

$$\cos(4\phi) = 4\alpha - 3, \quad \cos(2\theta) = \frac{\alpha - 1 \pm \frac{2}{\sqrt{7}}\sqrt{5 - 2\alpha}}{\alpha + 1}, \quad \alpha \in [1/2, 1]. \quad (\text{S5})$$

In general, the orbit of the restricted Clifford group is not a 4-design even if the spherical angles θ, ϕ satisfy Eq. (S5). Here we are particularly interested in the special value $\alpha = 1$, which means

$$\phi = 0, \quad \theta = \frac{1}{2} \arccos \sqrt{\frac{3}{7}}. \quad (\text{S6})$$

The corresponding Bloch vector reads

$$(r_1, r_2, r_3) = \left(-\sqrt{\frac{1}{2} - \frac{1}{2}\sqrt{\frac{3}{7}}}, 0, \sqrt{\frac{1}{2} + \frac{1}{2}\sqrt{\frac{3}{7}}} \right). \quad (\text{S7})$$

Up to overall phase factors, the stabilizer of the fiducial state within the Clifford group consists of the three unitary operators $I \otimes I, HPZ \otimes I, HPHPX \otimes I$, and the orbit length is 3840. By contrast, the stabilizer within the restricted Clifford group is trivial, and the orbit length is 960. Surprisingly, the orbit generated by the restricted Clifford group also forms a 4-design, although the restricted Clifford group is only a 2-design [4]. This result can be verified by direct calculation based on the t th frame potential with $t = 4$ [see Eq. (S8) below]. This 4-design is appealing to experimental realization because it has a small cardinality.

S3. NUMERICAL GENERATION OF 4-DESIGNS

The t th frame potential of a set of K states $\{|\psi_j\rangle\}_j$ is defined as [7–9]

$$\Phi_t(\{|\psi_j\rangle\}_j) = \frac{1}{K^2} \sum_{j,k} |\langle \psi_j | \psi_k \rangle|^{2t}. \quad (\text{S8})$$

It satisfies the inequality

$$\Phi_t(\{|\psi_j\rangle\}_j) \geq \frac{1}{D_t}, \quad (\text{S9})$$

and the lower bound is saturated iff the set $\{|\psi_j\rangle\}_j$ forms a t -design. This result is particularly convenient to determining whether a set forms a t -design or not. Moreover, given an initial set of states, better and better approximate t -designs can be constructed by minimizing the t th frame potential. A concrete optimization algorithm is provided in Refs. [10, 11]. By virtue of this algorithm (with iteration number $k = 2 \times 10^6$ and random seed number $s = 10^5$) we generated an approximate numerical 4-design composed of 200 states in dimension 4. The corresponding frame potential is 0.02859873, which is 0.1% larger than the lower bound $1/35 = 0.02857143$. The ratio between the smallest and largest eigenvalues (within the symmetric subspace) of the moment operator $\sum_j (|\psi_j\rangle\langle\psi_j|)^{\otimes 4}$ is about 0.90. Although this figure of merit is not so close to the ideal value of 1, the numerical 4-design is accurate enough for our purpose according to the following analysis; cf. Figs. 3, 4 and Table II in the main text as well as Sec. S4 in this Supplemental Material.

If the state ensemble forms an ideal 4-design, then the estimation fidelity of the POVM $\mathcal{A} = \{A_j\}_j$ is determined by Eqs. (1) and (2) in the main text. Since the numerical 4-design is not ideal, to determine the optimal estimation fidelity $Q(A_j)$ in Eq. (2) should be replaced by

$$Q'(A_j) := (N+1)! \text{tr}_{1,\dots,N} [P'_{N+1}(A_j \otimes 1)], \quad (\text{S10})$$

where

$$P'_{N+1} = \frac{D_{N+1}}{K} \sum_j (|\psi_j\rangle\langle\psi_j|)^{\otimes 4}. \quad (\text{S11})$$

Accordingly, the optimal estimator should be supported in the eigenspace of $Q'(A_j)$ with the largest eigenvalue. Figure S1 shows the optimal estimation fidelities of 18 triples of MUB based on the numerical 4-design in comparison with the ideal values based on an exact 4-design. The maximal deviation from the ideal estimation fidelity is only 0.00053, which is much smaller than the maximal difference between estimation fidelities of inequivalent MUB. If instead we use the standard estimator supported in the eigenspace of $Q(A_j)$ with the largest eigenvalue (which is suboptimal), then the estimation fidelity that can be achieved is slightly smaller, but still close to the ideal value, as illustrated in Fig. S1. In this case, the maximal deviation from the ideal estimation fidelity is only 0.00027. These results show that the numerical 4-design is accurate enough for distinguishing inequivalent MUB.

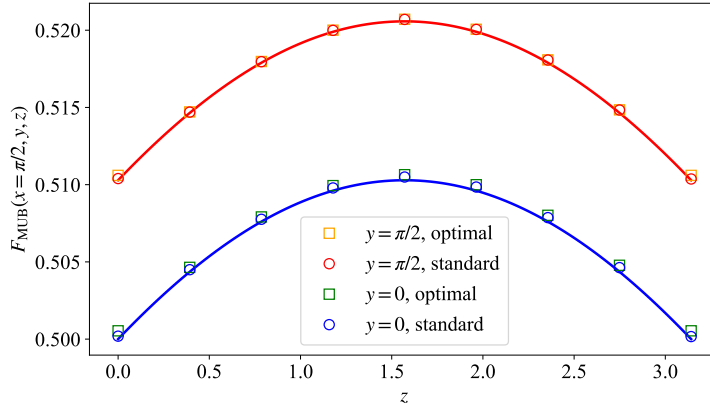


FIG. S1. The optimal and standard estimation fidelities of 18 triples of MUB based on the numerical 4-design in comparison with the ideal values (solid lines).

S4. EXPERIMENTAL IMPLEMENTATION OF THE TARGET PROJECTIVE MEASUREMENTS

In this section, we show how the measurement module in Fig.1 in the maintext (also shown in Fig. S2) performs the target projective measurements \mathcal{A} , \mathcal{B} , and \mathcal{C} associated with the triple of MUB corresponding to the parameter point (x, y, z) . The polarization (horizontal $|H\rangle$ and vertical $|V\rangle$) and the path (up $|\uparrow\rangle$ and down $|\downarrow\rangle$) degrees of freedom of a single photon act as a ququad. The submodule in the dashed box composed of two BDs and three HWPs set at 45° , 0° , and 45° implements the unitary transformation $(\text{NOT} \otimes \text{I})\text{SWAP}$, where NOT, I, and SWAP refer to the NOT gate, identity gate, and SWAP gate between the polarization and path qubits. The rotation angles of the other wave plates are specified in the embedded table. To verify the validity of the setup, the evolution of the basis states of \mathcal{A} , \mathcal{B} , and \mathcal{C} , i.e., $|\alpha_j\rangle$, $|\beta_k\rangle$, and $|\gamma_l\rangle$ for $j, k, l \in \{1, 2, 3, 4\}$ is summarized in Table S1.

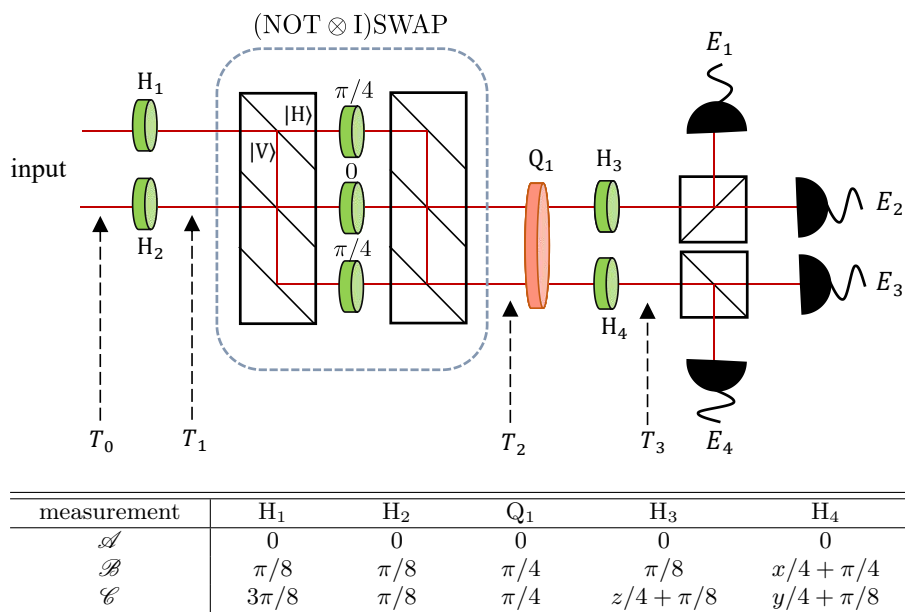


FIG. S2. Experimental realization of the projective measurements \mathcal{A} , \mathcal{B} , and \mathcal{C} associated with the triple of MUB corresponding to the parameter point (x, y, z) . The rotation angles of the relevant wave plates outside the dashed box are specified in the embedded table.

TABLE S1. The evolution of the basis states associated with the projective measurements \mathcal{A} , \mathcal{B} , and \mathcal{C} from time T_0 to time T_3 as indicated in Fig. S2 and the corresponding measurement outcomes.

input	T_0	T_1	T_2	T_3	outcome
$ \alpha_1\rangle$	$ H\rangle \uparrow\rangle$	$ H\rangle \uparrow\rangle$	$ V\rangle \uparrow\rangle$	$ V\rangle \uparrow\rangle$	E_1
$ \alpha_2\rangle$	$ H\rangle \downarrow\rangle$	$ H\rangle \downarrow\rangle$	$ H\rangle \uparrow\rangle$	$ H\rangle \uparrow\rangle$	E_2
$ \alpha_3\rangle$	$ V\rangle \uparrow\rangle$	$ V\rangle \uparrow\rangle$	$ V\rangle \downarrow\rangle$	$ V\rangle \downarrow\rangle$	E_4
$ \alpha_4\rangle$	$ V\rangle \downarrow\rangle$	$ V\rangle \downarrow\rangle$	$ H\rangle \downarrow\rangle$	$ H\rangle \downarrow\rangle$	E_3
$ \beta_1\rangle$	$\frac{1}{2}(H\rangle + V\rangle)(\uparrow\rangle + \downarrow\rangle)$	$\frac{1}{\sqrt{2}} H\rangle(\uparrow\rangle + \downarrow\rangle)$	$\frac{1}{\sqrt{2}}(H\rangle + V\rangle) \uparrow\rangle$	$ H\rangle \uparrow\rangle$	E_2
$ \beta_2\rangle$	$\frac{1}{2}(H\rangle - V\rangle)(\uparrow\rangle + ie^{ix} \downarrow\rangle)$	$\frac{1}{\sqrt{2}} V\rangle(\uparrow\rangle + ie^{ix} \downarrow\rangle)$	$\frac{1}{\sqrt{2}}(ie^{ix} H\rangle + V\rangle) \downarrow\rangle$	$ H\rangle \downarrow\rangle$	E_3
$ \beta_3\rangle$	$\frac{1}{2}(H\rangle + V\rangle)(\uparrow\rangle - \downarrow\rangle)$	$\frac{1}{\sqrt{2}} H\rangle(\uparrow\rangle - \downarrow\rangle)$	$\frac{1}{\sqrt{2}}(- H\rangle + V\rangle) \uparrow\rangle$	$ V\rangle \uparrow\rangle$	E_1
$ \beta_4\rangle$	$\frac{1}{2}(H\rangle - V\rangle)(\uparrow\rangle - ie^{ix} \downarrow\rangle)$	$\frac{1}{\sqrt{2}} V\rangle(\uparrow\rangle - ie^{ix} \downarrow\rangle)$	$\frac{1}{\sqrt{2}}(-ie^{ix} H\rangle + V\rangle) \downarrow\rangle$	$ V\rangle \downarrow\rangle$	E_4
$ \gamma_1\rangle$	$\frac{1}{2}[(H\rangle + V\rangle) \uparrow\rangle - e^{iy}(H\rangle - V\rangle) \downarrow\rangle]$	$\frac{1}{\sqrt{2}} V\rangle(\uparrow\rangle - e^{iy} \downarrow\rangle)$	$\frac{1}{\sqrt{2}}(-e^{iy} H\rangle + V\rangle) \downarrow\rangle$	$ V\rangle \downarrow\rangle$	E_4
$ \gamma_2\rangle$	$\frac{1}{2}[(H\rangle - V\rangle) \uparrow\rangle + e^{iz}(H\rangle + V\rangle) \downarrow\rangle]$	$\frac{1}{\sqrt{2}} H\rangle(\uparrow\rangle - e^{iz} \downarrow\rangle)$	$\frac{1}{\sqrt{2}}(e^{iz} H\rangle - V\rangle) \uparrow\rangle$	$ V\rangle \uparrow\rangle$	E_1
$ \gamma_3\rangle$	$\frac{1}{2}[(H\rangle + V\rangle) \uparrow\rangle + e^{iy}(H\rangle - V\rangle) \downarrow\rangle]$	$\frac{1}{\sqrt{2}} V\rangle(\uparrow\rangle + e^{iy} \downarrow\rangle)$	$\frac{1}{\sqrt{2}}(e^{iy} H\rangle + V\rangle) \downarrow\rangle$	$ H\rangle \downarrow\rangle$	E_3
$ \gamma_4\rangle$	$\frac{1}{2}[(H\rangle - V\rangle) \uparrow\rangle - e^{iz}(H\rangle + V\rangle) \downarrow\rangle]$	$\frac{1}{\sqrt{2}} H\rangle(\uparrow\rangle + e^{iz} \downarrow\rangle)$	$\frac{1}{\sqrt{2}}(e^{iz} H\rangle + V\rangle) \uparrow\rangle$	$ H\rangle \uparrow\rangle$	E_2

S5. ESTIMATION FIDELITIES OF EQUIVALENT MUB

Here we provide some auxiliary results on the three-copy estimation fidelities of equivalent MUB in dimension 4. We start with the triple of MUB corresponding to the parameter point $x = y = z = \pi/2$ and apply the controlled phase gate $\text{diag}(1, 1, 1, e^{i\phi})$ on the three bases simultaneously. If the state ensemble forms an ideal 4-design, which is the case for the Clifford 4-design, then the exact estimation probability is equal to $(46 + 5\sqrt{3})/105 \simeq 0.52057$, which is invariant under any unitary transformation of the MUB, as illustrated in plot (a) in Fig. S3. This plot also shows the estimation fidelity together with the standard deviation determined by numerical simulation with each measurement repeated 10000×10 times. The statistical fluctuation causes a small variation of the estimation fidelity with ϕ , whose order of magnitude is around 10^{-4} .

If the Clifford 4-design is replaced by the numerical 4-design, then even the exact estimation fidelity may depend on the phase as illustrated in plot (b) in Fig. S3. Fortunately, this variation is even smaller than the one induced by statistical fluctuation and is negligible compared with the maximal difference between estimation fidelities of inequivalent MUB.

TABLE S2. Exact and simulated three-copy estimation fidelities of equivalent MUB constructed by applying 10000 random unitaries to the MUB corresponding to the parameter point $x = y = z = \pi/2$. Also shown are the standard deviations and maximal deviations over the random unitaries. In numerical simulation, each measurement is repeated 10000×10 times. The state ensemble corresponds to either the Clifford 4-design or the numerical 4-design.

4-design	exact estimation fidelity					simulated estimation fidelity				
	maximal	minimal	average	std.	maximal deviation	maximal	minimal	average	std.	maximal deviation
Clifford	0.52057	0.52057	0.52057	0	0	0.52080	0.52025	0.52057	0.00006	0.00032
numerical	0.52083	0.52030	0.52057	0.00007	0.00027	0.52123	0.51995	0.52057	0.00016	0.00066

Next, we consider the impact of random unitary transformations instead of the controlled phase gate on the triple of MUB corresponding to the parameter point $x = y = z = \pi/2$. In total 10000 random unitaries are generated and applied. Table S2 summarizes the maximal, minimal, and average estimation fidelities together with the standard deviations and maximal deviations based on the Clifford 4-design and numerical 4-design, respectively. Again, the deviations are much smaller than the maximal difference between estimation fidelities of inequivalent MUB. For the

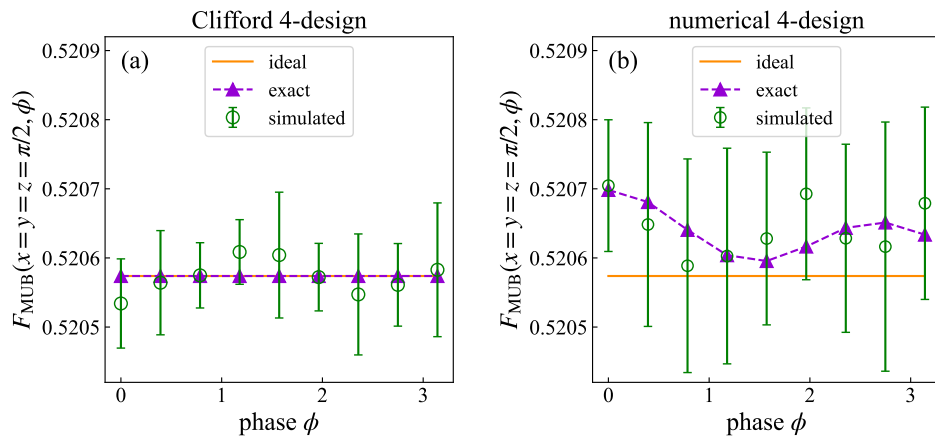


FIG. S3. Exact and simulated three-copy estimation fidelities of equivalent MUB constructed by applying the controlled-phase gate $\text{diag}(1, 1, 1, e^{i\phi})$ to the MUB corresponding to the parameter point $x = y = z = \pi/2$. In numerical simulation, each measurement is repeated 10000×10 times. The state ensemble corresponds to the Clifford 4-design in plot (a) and numerical 4-design in plot (b).

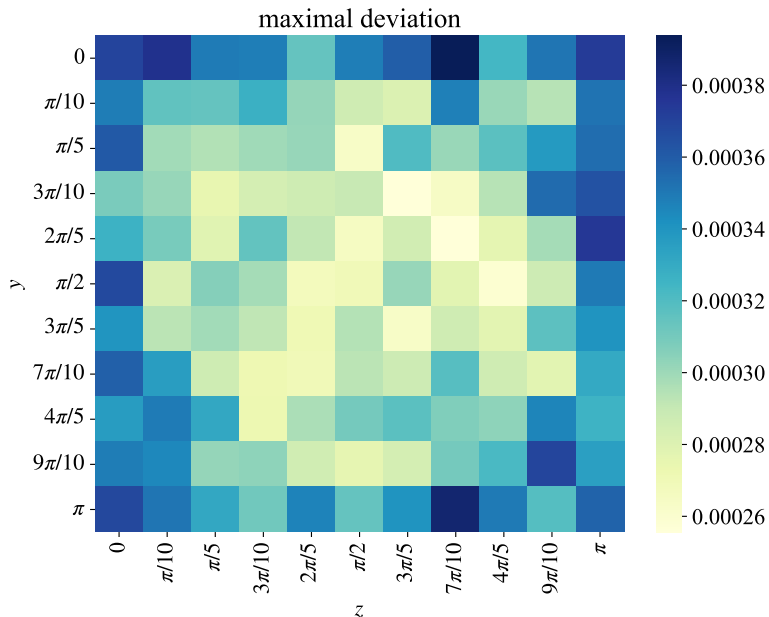


FIG. S4. Maximal deviations of the exact three-copy estimation fidelities (from the ideal values) of equivalent MUB constructed by applying 10000 random unitaries to MUB corresponding to the $y - z$ plane with $x = \pi/2$. The state ensemble corresponds to the numerical 4-design.

numerical 4-design, Fig. S4 further shows the maximal deviations between the exact estimation fidelities and the ideal estimation fidelities for MUB corresponding to the $y - z$ plane with $x = \pi/2$. The order of magnitude is similar to the counterpart in Table S2.

S6. ESTIMATION FIDELITIES BASED ON RANDOM SUBSETS OF THE CLIFFORD 4-DESIGN

In the maintext we determined the estimation fidelities of triples of MUB by averaging over all states in the Clifford 4-design. Here we consider alternative approaches by averaging over random subsets of the Clifford 4-design. To this end, we randomly select K distinct states from the Clifford 4-design and compute the estimation fidelity $F_{\text{MUB}}(x, y, z)$

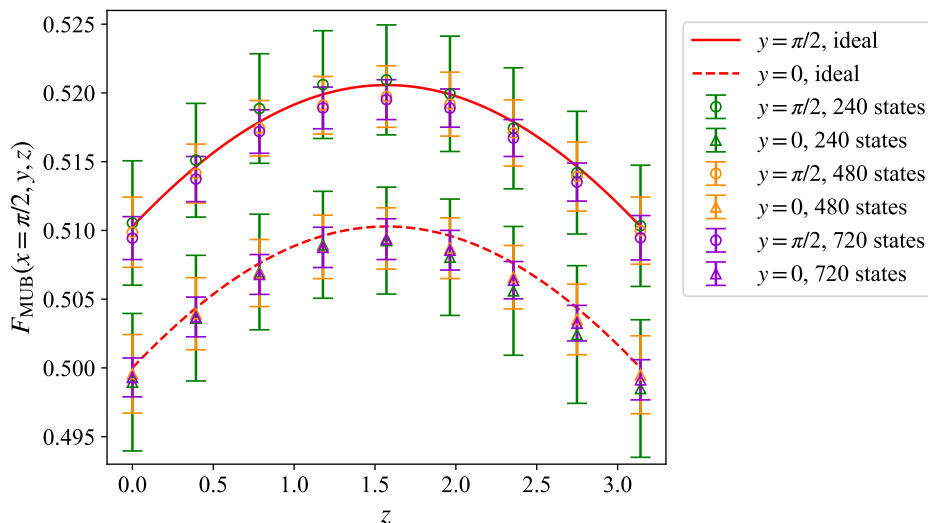


FIG. S5. Estimation fidelities $F_{\text{MUB}}(x, y, z)$ based on random subsets of the Clifford 4-design with 240, 480, and 720 states, respectively. Each data point is an average over 30 selections sampled from the experimental data. The error bar indicates the standard deviation over the 30 selections. The ideal estimation fidelity is also plotted for comparison.

TABLE S3. Estimation fidelities $F_{\text{MUB}}(x, y, z)$ based on random subsets of the Clifford 4-design with 240, 480, and 720 states, respectively. Each data point is an average over 30 selections sampled from the experimental data. The error bar indicates the standard deviation over the 30 selections. The ideal estimation fidelity and experimental estimation fidelity based on all 960 states of the Clifford 4-design are also shown for comparison.

z		0	$\frac{\pi}{8}$	$\frac{\pi}{4}$	$\frac{3\pi}{8}$	$\frac{\pi}{2}$	$\frac{5\pi}{8}$	$\frac{3\pi}{4}$	$\frac{7\pi}{8}$	π
$x = \frac{\pi}{2}$	240	0.5105(45)	0.5151(41)	0.5189(40)	0.5206(39)	0.5209(40)	0.5199(42)	0.5174(44)	0.5142(45)	0.5103(44)
	480	0.5099(26)	0.5141(21)	0.5174(20)	0.5191(21)	0.5197(22)	0.5192(23)	0.5171(24)	0.5139(25)	0.5100(24)
	$y = \frac{\pi}{2}$ 720	0.5094(16)	0.5137(16)	0.5172(16)	0.5189(15)	0.5195(15)	0.5189(14)	0.5167(13)	0.5135(14)	0.5095(16)
	960	0.5096	0.5137	0.5172	0.5190	0.5197	0.5192	0.5171	0.5139	0.5096
	ideal	0.5103	0.5146	0.5179	0.5199	0.5206	0.5199	0.5179	0.5146	0.5103
$x = \frac{\pi}{2}$	240	0.4990(50)	0.5036(46)	0.5070(42)	0.5090(39)	0.5093(39)	0.5081(42)	0.5056(47)	0.5024(50)	0.4985(50)
	480	0.4996(29)	0.5039(26)	0.5069(24)	0.5088(23)	0.5094(22)	0.5087(22)	0.5066(23)	0.5035(26)	0.4995(28)
	$y = 0$ 720	0.4993(14)	0.5037(14)	0.5068(14)	0.5088(15)	0.5094(15)	0.5086(14)	0.5064(14)	0.5033(13)	0.4991(15)
	960	0.4994	0.5036	0.5068	0.5088	0.5095	0.5088	0.5067	0.5036	0.4992
	ideal	0.5000	0.5044	0.5076	0.5096	0.5103	0.5096	0.5076	0.5044	0.5000

for each triple of MUB by averaging over the experimental data (the average frequency of each outcome determined by 10000×10 measurements) corresponding to the K states. This procedure is repeated 30 times to determine the mean estimation fidelity and the standard deviation. The main results for $K = 240, 480, 720$ are illustrated in Fig. S5 and summarized in Table S3. For all three choices, the mean estimation fidelities thus determined are close to the ideal value based on the Clifford 4-design. Moreover, the standard deviation tends to decrease monotonically as K increases as expected.

-
- [1] B. Bolt, T. G. Room, and G. E. Wall, On the Clifford collineation, transform and similarity groups. I., Journal of the Australian Mathematical Society **2**, 60–79 (1961).
[2] B. Bolt, T. G. Room, and G. E. Wall, On the Clifford collineation, transform and similarity groups. II., Journal of the Australian Mathematical Society **2**, 80–96 (1961).

- [3] D. Gottesman, Stabilizer codes and quantum error correction (1997), arXiv:quant-ph/9705052.
- [4] H. Zhu, Multiqubit Clifford groups are unitary 3-designs, Phys. Rev. A **96**, 062336 (2017).
- [5] Z. Webb, The Clifford group forms a unitary 3-design, Quantum Info. Comput. **16**, 1379–1400 (2016).
- [6] H. Zhu, R. Kueng, M. Grassl, and D. Gross, The Clifford group fails gracefully to be a unitary 4-design (2016), arXiv:1609.08172.
- [7] J. M. Renes, R. Blume-Kohout, A. J. Scott, and C. M. Caves, Symmetric informationally complete quantum measurements, J. Math. Phys. **45**, 2171 (2004).
- [8] G. Zauner, Quantum designs: Foundations of a noncommutative design theory, Int. J. Quantum Inf. **09**, 445 (2011).
- [9] A. J. Scott, Tight informationally complete quantum measurements, J. Phys. A: Math. Gen. **39**, 13507 (2006).
- [10] D. Hughes and S. Waldron, Spherical (t, t) -designs with a small number of vectors, Linear Algebra and its Applications **608**, 84 (2021).
- [11] A. Elzenaar, <https://github.com/aelzenaar/tightframes>.